

# FINE RESOLUTION ESTIMATION OF THE FUTURE URBAN HEAT ISLAND EFFECT FOR BUDAPEST

Project No. K120605

Final Report

2016-2023

The urban heat island (UHI) effect is probably the most often analyzed environmental phenomenon of large cities. We aim to use different approaches to evaluate the UHI effect of the agglomeration around the Hungarian Capital, Budapest. The city is divided by the river Danube into the hilly, greener Buda side on the west, and the flat, more densely built-up Pest side on the east. This research project analyzes measurements (both in-situ and satellite) as well, as mesoscale modeling of the target area.

## 1. Measurement campaigns for air temperature

One of the target areas within the city is the district IX (called Ferencváros, Fig. 1), where several block rehabilitation programs have been completed in the recent decades, which resulted in functional and structural changes of special subsections of the district.

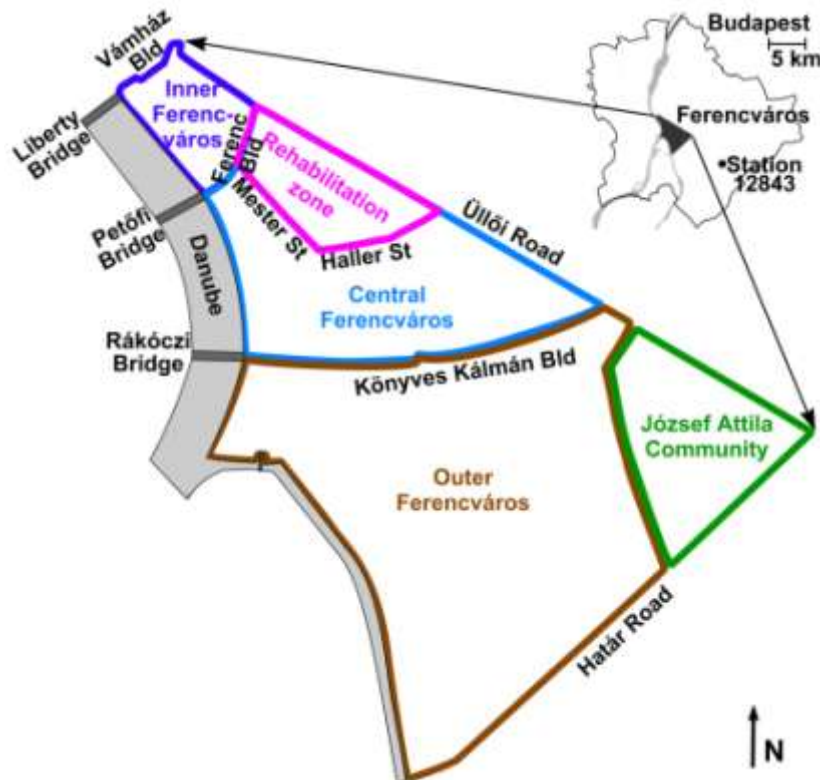


Fig. 1: Geographical location of the target district in Budapest, Hungary

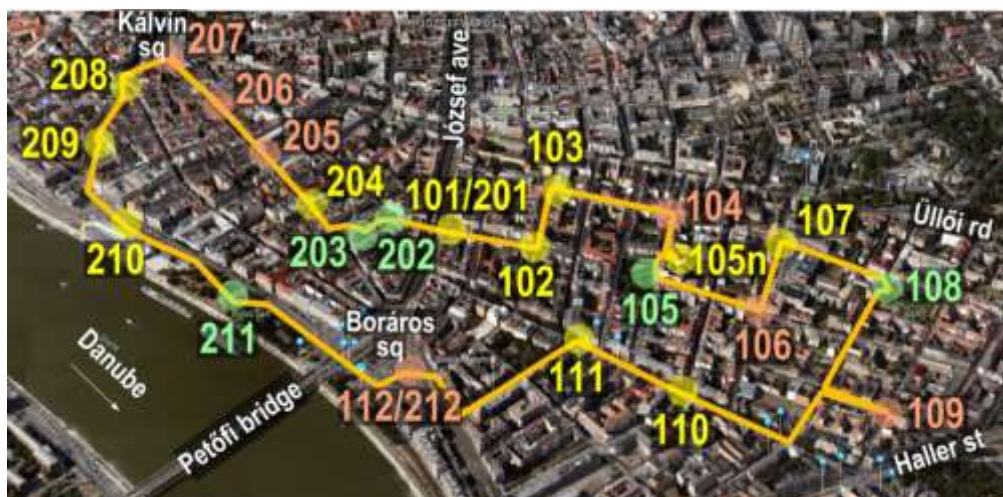
Ferencváros is located near the river Danube in the southern central part of Budapest, which is very heterogeneous and consists of 3- and 4-storey old buildings, block houses with either 4 or 8 levels, brown industrial areas, and large areas occupied by the railways system. Partly due to the functional and structural changes of the special subsections of the district substantial local climatic changes occurred in the past few decades. Concentrated efforts of the local government completed several block rehabilitation programs starting from the 1980s. Since 1993 in the most densely built inner part of the district entire blocks were renovated and modified in order to create more livable environment for the citizens. Altogether 220 houses (with ~1300 apartments) were demolished with new buildings were built in their places, 49 houses (with ~1050 apartments) were renovated (LGF, 2010). Within the framework of the block rehabilitation programs the inner parts of the blocks were demolished, thus, inside the blocks more common green areas could be created. Moreover, several parks have been enlarged, and small green areas have been created along the streets.

We completed several measuring campaigns with 24-hour continuous in-situ measurements of temperature and humidity in Inner and Central Ferencváros including the rehabilitation zone of the district IX of Budapest during different weather conditions and different seasons. The measuring program started in the early spring of 2015. The measurements were scheduled once a week from 2 p.m. on Thursdays to 2 p.m. on Fridays. In addition, summer campaigns (in July 2016, 2017, 2018) covered at least 72 hours continuously. The on-going measuring program involves BSc students specialized in Earth sciences and MSc students specialized in meteorology. Altogether 77 days with more than 850 hours of measurements were collected. Air temperature and relative humidity were recorded with Testo-623 instruments (Fig. 2) along a pre-defined route consisting of 23 measuring points (Fig. 3), which covers the studied area.



Fig. 2: The complex measuring instrument Testo-623 with data logger

The measuring sites were selected at different representative points of the district, such as green parks, narrow streets, paved squares and roads (Pongrácz et al., 2016). The whole measuring route is divided into two parts, where the measurements are recorded simultaneously (from 101 to 112, and 201 to 212 with the identical starting and ending sites, i.e., 101 is identical to 201, and 112 is 212) lasting about 1-1.5 hours. Then, the measurements are recorded along the same two routes but in reverse order (i.e., starting from 112/212, and ending at 101/201). In order to temporally adjust the measurements, two records from the consequent (and reversed) partial paths are averaged over each site resulting in an average value being representative for a virtual time. More precisely, since the moving speeds between sites and the distances between sites are not perfectly identical, this virtual time is given as a 10-20 minute time period. For calculating the UHI intensity, temperature measurements were compared to the hourly recorded data of the Budapest synoptic station (ID number: 12843) located in the southeastern suburb district of the city (shown in Fig. 1). Similarly, difference between relative humidity measurements were also calculated and analyzed.



- |                              |                                |
|------------------------------|--------------------------------|
| 201: Ferenc bld. / Tompa st. | 101: Ferenc bld. / Tompa st.   |
| 202: Bakáts sq. / Tompa st.  | 102: Tompa st. / Liliom st.    |
| 203: Bakáts sq. / Ráday st.  | 103: Liliom st. / Tűzoltó st.  |
| 204: Ráday st. 42            | 104: Tűzoltó st. / Bokréta st. |
| 205: Ráday st. / Biblia st.  | 105: Ferenc sq.                |
| 206: Ráday/Erkel st          | 105n: Passage                  |
| 207: Kálvin sq.              | 106: Balázs st. / Thaly st.    |
| 208: Lónyay st. / Gönczy st. | 107: Univ. Building            |
| 209: Csarnok sq.             | 108: Kerekerdő Park            |
| 210: Building Bálna          | 109: Márton st./ Gát st.       |
| 211: Nehru Park              | 110: Mester st. / Viola st.    |
| 212: Boráros sq.             | 111: Mester st. / Tinódi st.   |
|                              | 112: Boráros sq.               |

Fig. 3: Measuring points along the predefined route.

First, some results from the summer campaign in 2016 (July 4–6) are shown in Figs. 4–5. The synoptic situation during the days of the measuring campaign was ideal to detect the UHI effect, namely, anticyclonic circulation over the Carpathian basin with >1020 hPa sea level pressure and clear sky conditions.

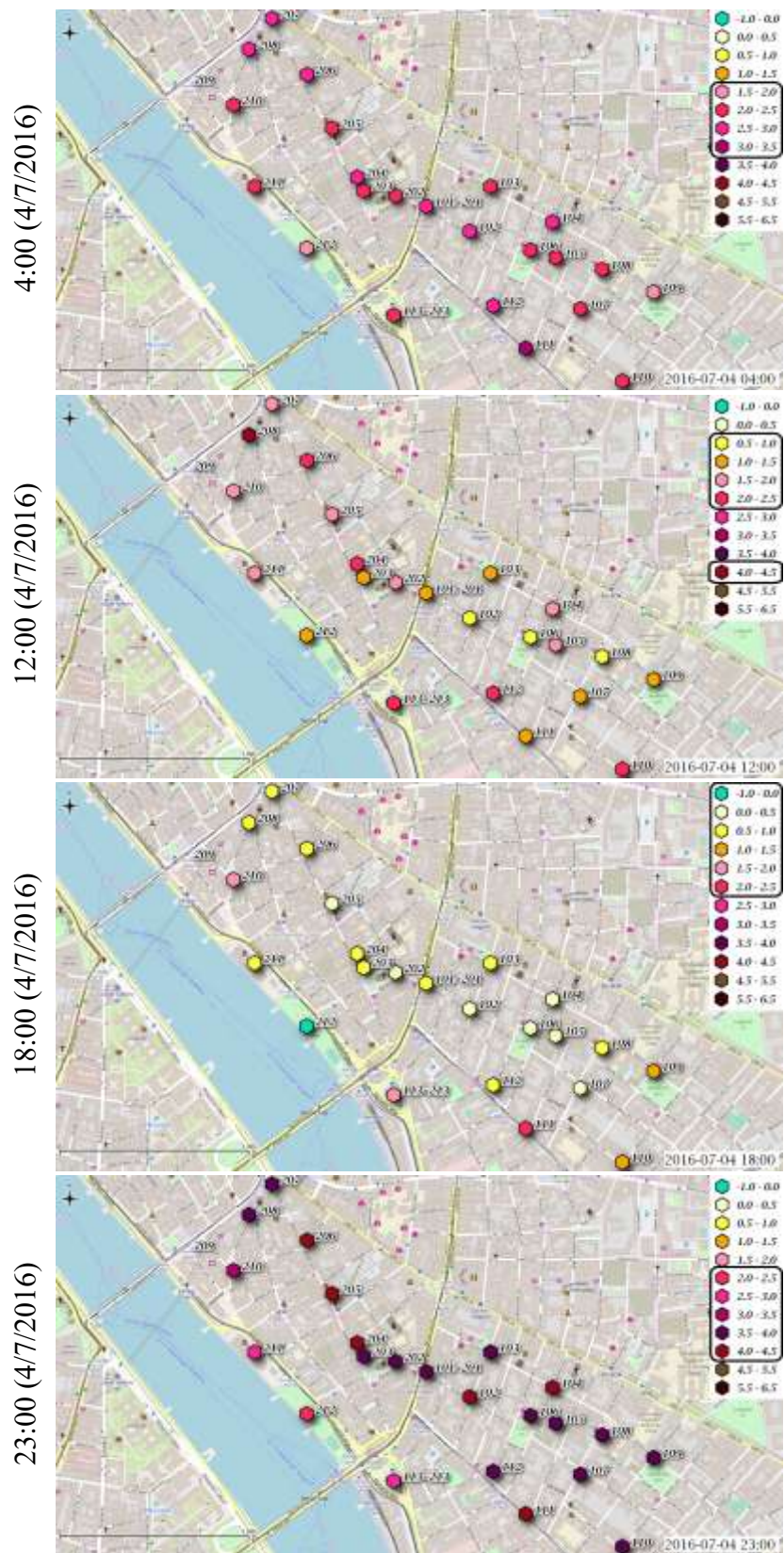


Fig. 4: The daily cycle of the spatial patterns of UHI intensity, 4 July 2016.

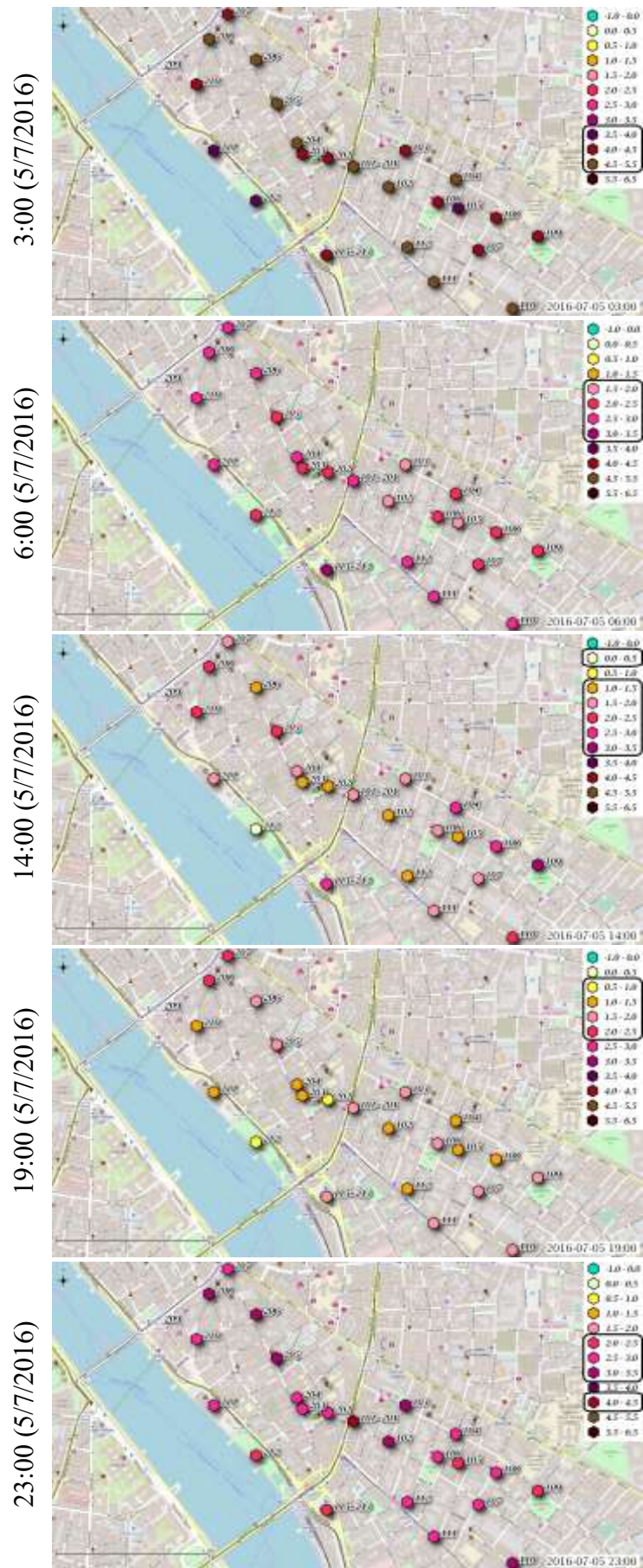


Fig. 5: The daily cycle of the spatial patterns of UHI intensity, 5 July 2016.

In addition to the spatial structure, a more detailed analysis of the daily cycle of UHI intensity is carried out. One example from the summer campaign in 2016 is shown in Fig. 6 for the measuring point 105n, which is located in a passage surrounded by buildings with a height of about 20 m, the vegetation cover is ~60% (Fig. 7).

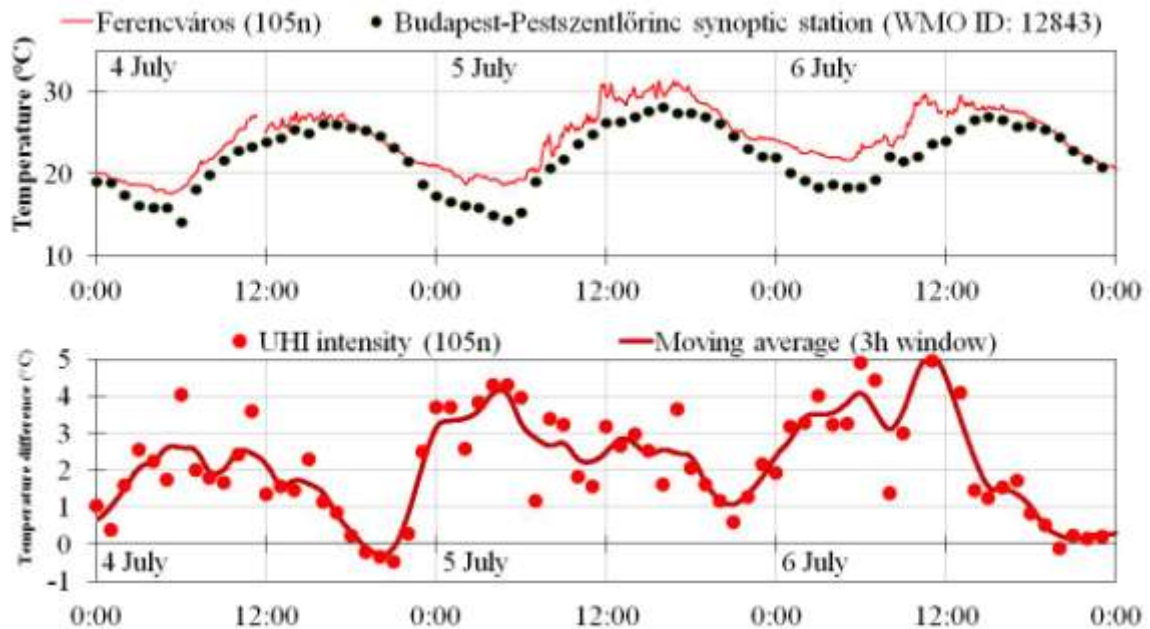


Fig. 6: The daily cycle of temperature measurements (at measuring site 105n compared to the synoptic station of Budapest, WMO ID: 12843), 4–6 July 2016



Fig. 7: Measuring site 105n

The graph of Fig. 6 clearly indicates that the measuring site in the inner city is warmer than the southeastern suburbs of Budapest. The greatest UHI intensity, which is defined as the difference between the temperatures of measuring site 105n and the suburban-located synoptic station of Budapest, was detected during night time, in some days closer to dawn.

On the basis of the measurements in different seasons the relationships between the UHI intensity values and various weather conditions are evaluated. The strongest relationships were found between the maximum UHI intensity and the cloud cover (Fig. 8), namely, intense UHI occurs in clear sky conditions, whereas the UHI effect becomes quite small when cloudy conditions occur.

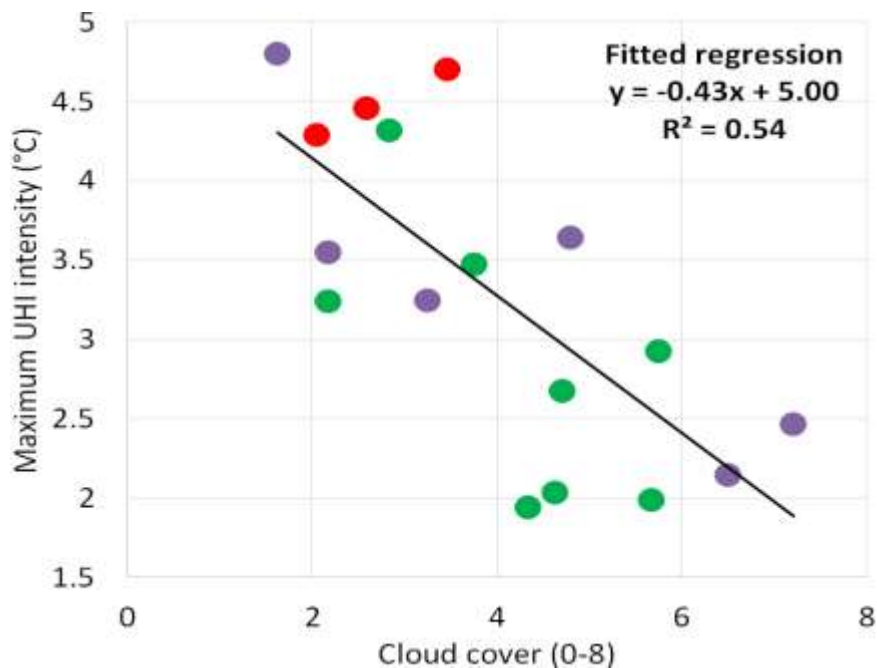


Fig. 8: Relationship between the maximum UHI intensity and cloud cover (2016-2018).

Although these measurements can be used to evaluate the temporal evolution of the UHI effect, they do not cover fully the agglomeration area. In order to provide a full spatial coverage of Budapest and its vicinity, satellite measurements serve as the basis of UHI analysis.

Major journal publications of these project results:

Dian Cs., Pongrácz R., Incze D., Bartholy J., Talamon A. (2019): Analysis of the urban heat island intensity based on air temperature measurements in a renovated part of Budapest (Hungary). *Geographica Pannonica*, Vol. 23 (No. 4), pp. 277–288 DOI: 10.5937/gp23-23839

Pongrácz R., Dian Cs., Incze D., Kurcsics M., Dezső Zs., Bartholy J. (2017): Budapesti városklimatológiai helyszíni mérések elemzése. *Léggör*, 62., No. 3. pp. 126-129. (in Hungarian)

## 2. Measurement campaigns for surface temperature

In the framework of the long-term cooperation between the Urban Climate Research Group of the Department of Meteorology at the Eötvös Loránd University (Budapest) and the Department of Environment at the Municipality of Újbuda (district XI of Budapest), regular urban climate measurements were carried out in the district XI of Budapest to detect the UHI effect on different spatial scales.

Measuring campaigns were conducted in July 2018 and later, in May and June 2019 to determine the surface temperature of various urban materials using an infrared thermometer. The purpose of these measurements was to obtain information about the thermal properties of different urban surfaces, objects (covering materials, walls, pavements, etc.) in order to analyse which surfaces are suitable for decreasing and hence mitigating the UHI effect. The impact of the colour of different surfaces and the role of shading are analysed as well.

Újbuda is one of the most dynamically developing districts of the Hungarian capital with more than 130,000 inhabitants (HMI, 2019). Overall, the 23 districts of Budapest have a total of 1,752,286 inhabitants, of which almost 8% live in Újbuda, thus forming the most populated district. The geographical location of the district and the measuring sites is presented in Fig. 9. The district is characterised by very diverse land use types: both densely and sparsely built-up residential areas, industrial and commercial areas, road and railway traffic nodes are present as well as parks, forests, lakes and rivers. Recently, major real estate developments have taken place in the district.



Fig. 9: Geographical location of Újbuda (District XI of Budapest) and the measuring sites. M indicates the Móricz Zsigmond Square (Artificial Covered Site), B indicates the Bikás Park (Green Park Site).

The measurements were made with a Voltcraft IR-280 infrared thermometer (Fig. 10), which has been designed for non-contact temperature measurement. This instrument determines the surface temperature of an object from its emitted infrared energy and its emissivity. The temperature measuring range is from  $-30\text{ }^{\circ}\text{C}$  to  $270\text{ }^{\circ}\text{C}$ .



Fig. 10: Voltcraft IR-280 infrared thermometer used for measuring surface temperature.

Our urban climate measurement campaigns were organised in the periods of high solar elevation angles, i.e. in late spring and early summer (more specifically, in July 2018, and in May and June 2019) at two measuring sites. The first site is the largest public park of the

district, called Bikás Park (Green Park Site), the second site is a busy transportation centre, one of the most densely built-up squares of the city, namely the Móricz Zsigmond Square (Artificial Covered Site). We selected 37 measuring points at the Green Park Site (Fig. 11), and 17 measuring points at the Artificial Covered Site (Fig. 12). The detailed list with the name and surface materials of these measuring points for both sites can be found in Table 1 and Table 2, respectively. The Green Park Site includes several types of surface cover, both natural and artificial surfaces. The Artificial Covered Site is less diverse in land cover types, and it is dominated by different artificial surface materials (i.e. concrete and asphalt).



Fig. 11: The locations of 37 measuring points (B1-B37) at Bikás Park (Google Earth, 07/2018).

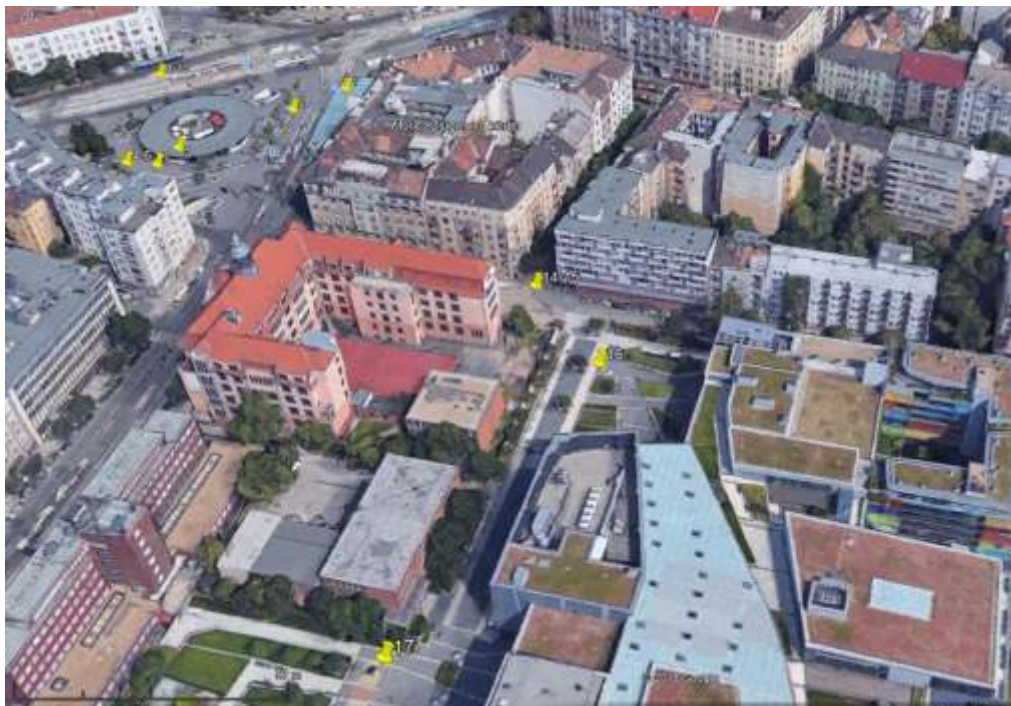


Fig. 12: The locations of 17 measuring points (M1-M17) at the Móricz Zsigmond Square (Google Earth, 07/2018).

Table 1. The list of measuring points and surface materials at Bikás Park

<b>number</b>	<b>description</b>	<b>surface material</b>
B1	market sign	concrete
B2	pillar in the market	metal
B3	subway station building	glass
B4	dark gray pavement blocks	concrete
B5	red pavement blocks	concrete
B6	gray pavement blocks	concrete
B7	dark gray pavement blocks	concrete
B8	light gray pavement blocks	concrete
B9	bench	wood
B10	bench	metal
B11	table	concrete
B12	statue of Grosics	metal
B13	lawn at the statue of Grosics	plant
B14	lawn under the tree	plant
B15	tree	plant
B16	red rubber paving	rubber+polyurethane
B17	red pavement	concrete
B18	reed	plant
B19	lake	water
B20	lake footbridge	wood
B21	gravel pavement	stone
B22	tree	plant
B23	bare soil	soil
B24	stony asphalt road	asphalt
B25	asphalt road	asphalt
B26	shrub	plant
B27	concrete building	concrete
B28	playground pavement	concrete
B29	statue of Bull	metal
B30	bare soil	soil
B31	grey rubber paving	rubber+polyurethane
B32	red rubber paving	rubber+polyurethane
B33	bicycle handlebars	plastic
B34	metal pipe	metal
B35	public workout equipment	metal
B36	tennis court cover	clay
B37	football field blue rubber paving	rubber+polyurethane

Table 2. The list of measuring points and surface materials at Móricz Zsigmond Square

number	description	surface material
M1	subway station building	glass
M2	bench	wood
M3	Bistro wall	concrete
M4	lawn	plant
M5	tree	plant
M6	reed	plant
M7	dark gray pavement blocks	concrete
M8	red pavement blocks	concrete
M9	blue pavement blocks	concrete
M10	gray pavement blocks	concrete
M11	handrail	plastic
M12	tram rail	metal
M13	asphalt pavement between tram rails	asphalt
M14	road	asphalt
M15	light gray pavement blocks	concrete
M16	bare soil at Allée shopping center	soil
M17	water surface at Allée shopping center	water

During the measurement campaign in 2018 (2–5 July), we carried out measurements four times per day at both sites: at 9 am, 1 pm, 5 pm and 9 pm. Weather conditions were ideal for our purposes with calm, clear, sunny weather, and the time of sunset was 8:43 pm. In the following year, three series of measurements were performed daily at 8 am, 2 pm, and 8 pm. The weather was cloudy with shorter sunny periods in some parts of the campaign. The sunset was recorded at 8:16 pm on 17 May, at 8:23–8:26 pm during 23–26 May, and at 8:36–8:37 during 6–7 June. We measured separately the temperature of the different surfaces exposed to direct sunlight and the temperature of the shaded surfaces if both types occurred at the measuring point. Hence, the role of direct sunlight in surface temperature can be examined.

The aims of this part of the project research were to evaluate and to compare the thermal properties of different typical surface covers within urban areas. For this purpose, common statistical tools were performed, i.e. box-and-whiskers diagrams to represent the distribution of surface temperature measurements over a specific surface cover, averaging available measurements to compare different types of surface covers, etc.

To study the thermal properties of various materials, first the mean surface temperature of the noon measurements is determined. Fig. 13 and Fig. 14 show the results for the Green Park Site and for the Artificial Covered Site, respectively. The upper part of the diagrams (positive direction) represents the average surface temperature values of the surfaces exposed to direct sunlight, while the bottom part (negative direction) shows the average temperatures of the shaded parts of the surfaces. In order to facilitate the comparison, different surface materials are represented by different colours. Both diagrams demonstrate clearly that the coolest surfaces are natural covers, i.e. water or vegetation. Even if the surface is exposed to direct sunlight, and thus, absorbs more radiation than from diffuse sunlight only, their surface temperature remains close to the values in case of shaded conditions (the temperature differences between the sunny and shaded surfaces are mostly around 5 °C). Bare soil warms up more than vegetation when exposed to direct solar radiation, so it is better to plant vegetation than to leave bare soil surface without any vegetation. The hottest surfaces are

clearly the sunny concrete pavements, dark painted wood objects, asphalt and rubber paving. Their average surface temperatures exceed 30 °C at noon, and even 40 °C in the case of wood, asphalt and rubber paving. The difference between mean temperatures of sunny and shaded surfaces of each measuring point depends on the properties of the actual surface material. Surface temperatures are relatively high, close to 30 °C, in the case of shaded concrete pavements, while direct solar radiation makes the surface temperatures of concrete higher, up to 30-40 °C. Temperature differences are greater for rubber-paved surfaces, namely, the mean temperatures in the shaded areas are between 20 °C and 30 °C, but these rubber surfaces become extremely hot (over 40 °C) when they are exposed to direct radiation.

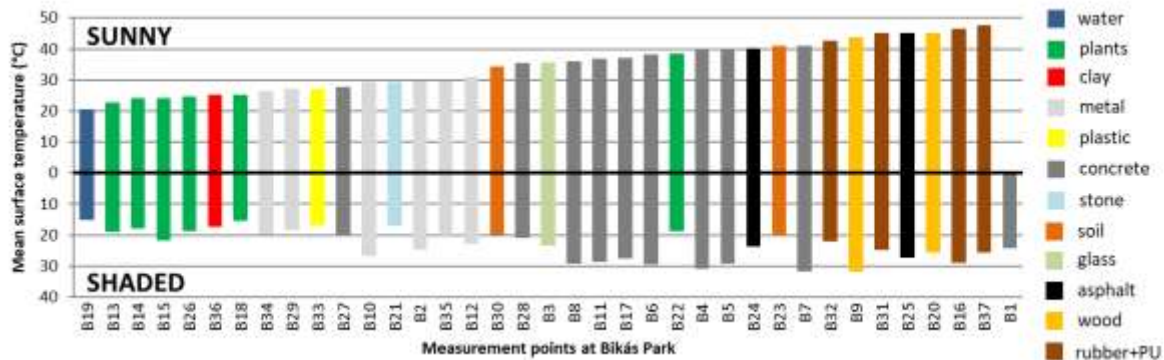


Fig. 13: Mean surface temperature of measurements around noon at measuring points in Bikás Park. Colours indicate the surface materials of the points. The upper part of the diagram (positive direction) represents the sunny, while the lower part (negative direction) represents the shaded measurements at the same point.

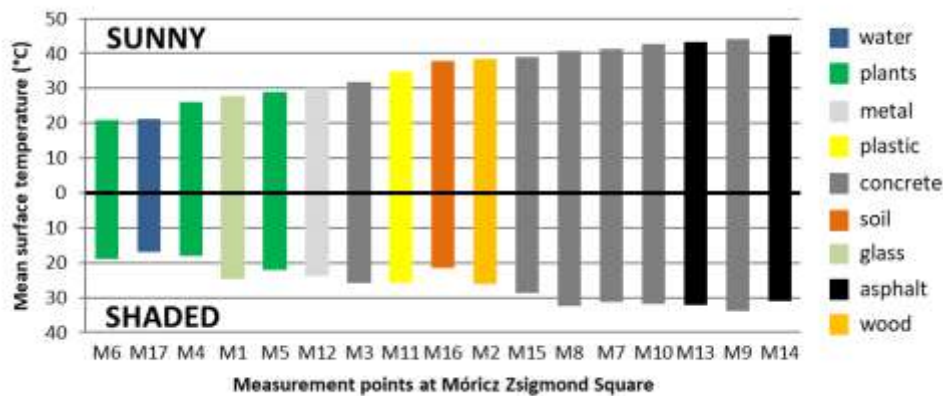


Fig. 14: Mean surface temperature of measurements around noon at measuring points in Móricz Zsigmond Square. Colours indicate the surface materials of the points. The upper part of the diagram (positive direction) represents the sunny, while the lower part (negative direction) represents the shaded measurements at the same point.

In the next steps of this study we focused on the thermal differences among the same types of surface covers, so we investigated the role of the colours in case of the concrete paving. For this purpose, four measuring points are selected from the Móricz Zsigmond Square that are close to each other with similar micro scale environments, but different colours. Measuring point M15 is covered by light grey pavement blocks, M10 is grey, M8 is red and M9 is blue. Fig. 15 compares the distribution of the surface temperature measurement

values of these selected points using a box-and-whisker diagram chart. (All available measurements are used in this analysis whether sunny or shaded.)

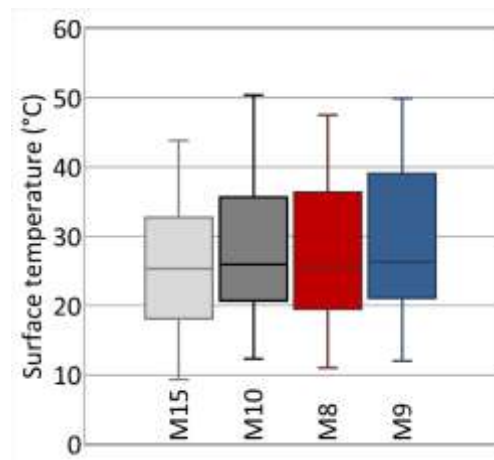


Fig. 15: Surface temperature distribution of concrete pavement surfaces of different colours at Móricz Zsigmond Square. The box-and-whisker diagram includes the minimum and the maximum (bottom and upper end of the whiskers, respectively), the lower and upper quartiles (bottom and top of the box, respectively) and the median (line inside the box) of all the available data. The colours of the pavement blocks: M15 – light grey, M10 – grey, M8 – red, M9 – blue.

The light grey pavement clearly shows the lowest temperature values, then, overall, the grey surface is warmer, the red is slightly warmer, and the blue pavement is the hottest. This sequence of temperature ranges clearly suggests that light coloured concrete covers are much better than dark coloured concrete covers from the point of view of how they affect the near-surface atmospheric layers where people can be found. The reason behind this behaviour is certainly the albedo (and consequently, the portions of reflected and absorbed radiations) of the different coloured concretes, i.e. light colours reflect more radiation than dark colours. As the temperature values of sunny surfaces are substantially higher than the temperature of shaded surfaces, the sub-median range of the entire distribution represents the shaded measurements, whereas the above-median range includes mainly the sunny measurements. Despite having more measurements for shaded conditions than sunny conditions, the asymmetry of the distribution shows a positive skewness towards higher temperature. This implies that the variation of sunny temperatures is greater than the variation of shaded temperatures.

As Fig. 13 shows, the hottest points in the measurement series are the rubber-paved surfaces exposed to direct radiation. This paving material has lately become very popular in the design of playgrounds, running tracks and sport fields. Various technologies exist for producing these types of surfaces; the most often-used technology consists of the following two main processes, (i) splitting small pieces of vulcanised rubber, and then, (ii) gluing them together with various polyurethane or latex materials. The use of these surfaces has several advantages. For instance, rubber-paved surfaces reduce the risk of injury, it is easy to keep them clean, and they have a modern look. However, from the urban climatological point of view, the use of these covers may also be disadvantageous due to their thermal properties. In addition, volatile organic compounds (VOCs) can be released from these surfaces, and the total emission flux is correlated to the track surface temperature (Chang et al., 1999).

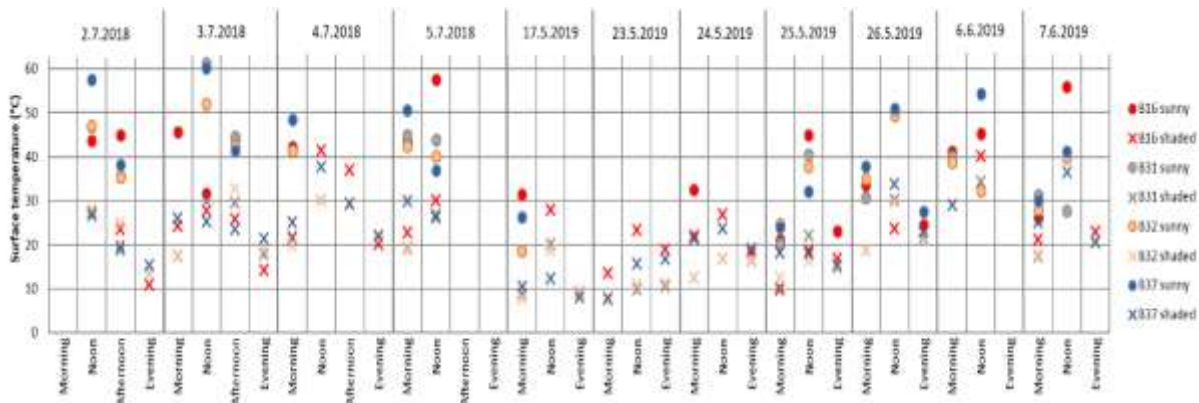


Fig. 16: Surface temperature measurements of different rubber-paved surfaces at Bikás Park measuring site. Circles and crosses represent temperatures at sunny and shaded points, respectively. The colours of the rubber surfaces are as follows:  
B16 – red, B31 – grey, B32 – red, B37 – blue.

In the last part of this study we focus on these rubber-paved surfaces to evaluate their behaviour in the measuring sites. Fig. 16 shows all temperature values for four measuring points covered by rubber paving located at Bikás Park (this surface cover type cannot be found at Móricz Zsigmond Square). The rubber paving materials are similar in these measuring points, but their colours are different, namely, B16 and B32 are red, B31 is grey, and B37 is blue. Sunny and shaded measurements are compared in this analysis, so different symbols are used for them in the diagram. Evening measurements mostly resulted in data for shaded conditions with very few exceptions. In addition, measurements with sunny conditions are missing on some days (e.g. 23.5.2019) due to cloudy weather. Summer is well-known for hot periods that can be even more severe in the urban environment. Extreme surface temperatures can appear during this period of the year, especially in calm, sunny weather conditions. The highest temperature of the present campaigns was measured on 3.7.2018 when the temperature of the grey rubber paving reached 61.2 °C shortly after noon. Fig. 16 clearly shows that there is a distinct difference between sunny and shaded surface temperature values. Shaded temperatures generally remain within tolerable temperature range, they exceed 30 °C in a few cases only. In contrast, sunny surfaces are often extremely warm (above 40 °C). These extreme temperatures have a negative impact on human comfort, so the usability of the facilities (playgrounds, sport fields) covered with this artificial material is strongly limited.

The main journal publication of these project results:

Dezső Zs., Pongrácz R., Bartholy J. (2019): Analysis of surface temperature measurements over complex urban sites. *Geographica Pannonica*, Vol. 23 (No. 4), pp. 337–346 DOI: 10.5937/gp23-23844

### 3. Analysis of satellite-based measurements

For the purpose of analyzing the entire spatial coverage of the Budapest agglomeration area, surface temperature is used, which is derived (Wan and Snyder, 1999) from the radiation data of 7 infrared channels (channel 20: 3660-3840 nm, channel 22: 3929-3989 nm, channel 23: 4020-4080 nm, channel 29: 8400-8700 nm, channel 31: 10780-11280 nm, channel 32:

11770-12270 nm, and channel 33: 13185-13485 nm) measured by the sensor MODIS<sup>1</sup> onboard satellites Terra (NASA, 1999) and Aqua (NASA, 2002).

MODIS is a cross-track scanning multi-spectral radiometer with 36 electromagnetic spectral bands from visible to thermal infrared. Horizontal resolution of the infrared measurements is 1 km. In the framework of EOS program numerous climatic and environmental parameters are determined using the raw radiation data. All the parameters are archived in universal format using 1200×1200 pixel tiles, they are available as validated, quality-controlled, geo-referenced, high-level datasets.

On the basis of error- and cloud-free parts of available surface temperature fields, SUHI (surface urban heat island) intensity values were calculated for 2001-2022 for each pixel within the 65×65 pixel representation of the Budapest agglomeration using the rural mean surface temperature LST (Bartholy et al., 2016).

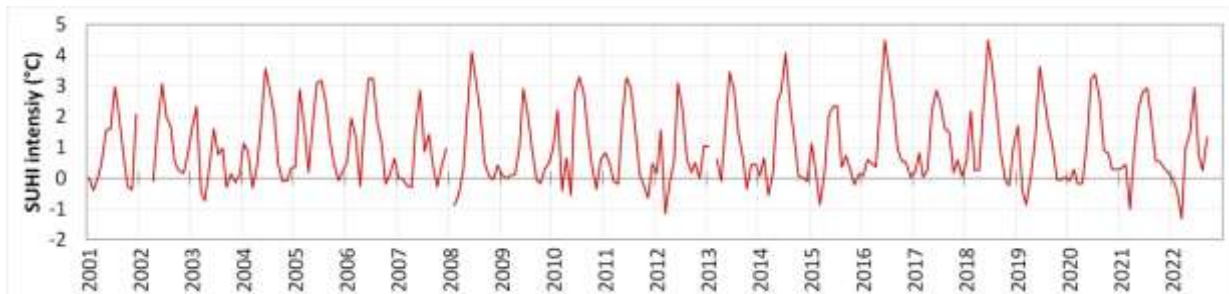


Fig. 17: The monthly mean SUHI intensity time series of Budapest on the basis of surface temperature determined from day-time Terra/MODIS measurements (2001-2022).

UHI results certainly differ when air temperature or surface temperature is taken into account. Fig. 17 shows the SUHI intensity time series of Budapest with maximum in summer (showing the structure in Fig. 18) and minimum in spring and late autumn (Pongrácz et al., 2010, 2016).

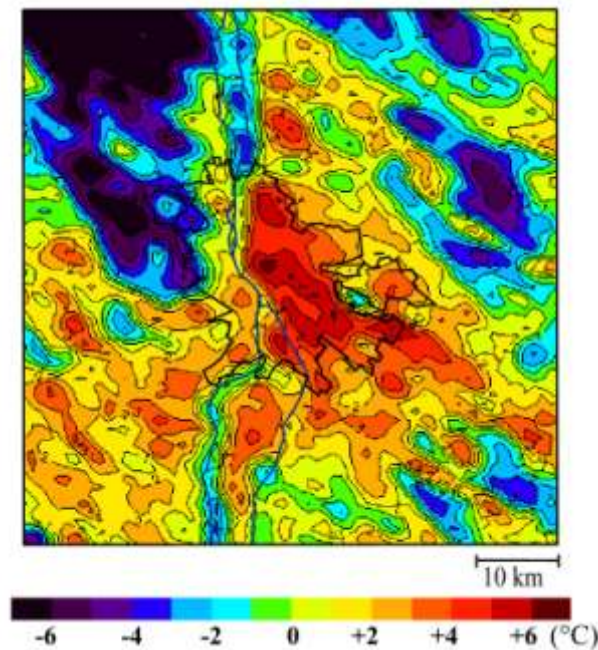


Fig. 18: The structure of the monthly mean SUHI intensity of Budapest on the basis of surface temperature determined from day-time Terra/MODIS measurements (June 2018).

<sup>1</sup> Moderate Resolution Imaging Spectroradiometer

Fig. 19 shows a case study for the evolution of SUHI intensity spatial structure in the  $70 \times 70 \text{ km}^2$  domain in August, when most of the cloudless days occur. A multi-center cyclone system was present in western and northern Europe, and an anticyclone dominated the weather in southern and central Europe. The air temperature was 30-35 °C in Hungary during the 4-day-long heat wave period.

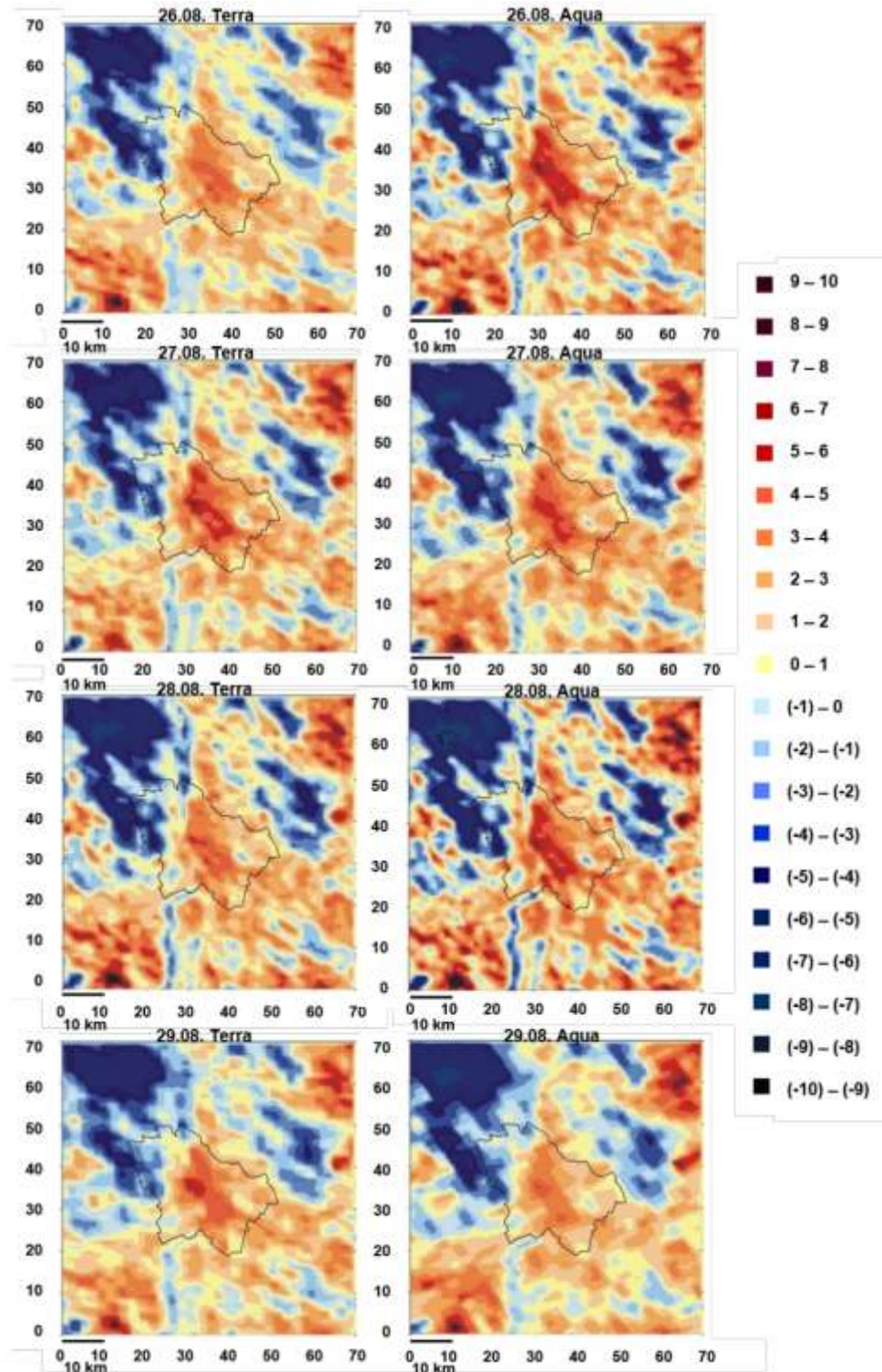


Fig. 19: Evolution of the SUHI intensity spatial structure based on Terra's morning (left) and Aqua's afternoon (right) measurements, 26-29 August 2016.

The highest SUHI intensities (7–8 °C) include the city center. Negative SUHI intensities occur in two main regions within the city: (i) the Danube, which flows through the city and the reason of the negative values is the different warming of water and land surface; (ii) the Buda Hills due to the forested coverage, and the height above sea level. The overall weather situation

Furthermore, we carried out the analysis of the connection of SUHI in Budapest to its Local Climate Zones (LCZ). Stewart and Oke (2012) defined the LCZ system. Seven parameters represent the geometry and surface cover properties (i.e. the sky view factor, aspect ratio, building surface fraction, impervious surface fraction, pervious surface fraction, height of roughness elements, terrain roughness class) and three parameters are used for thermal, radiative, and metabolic properties (i.e. surface admittance, surface albedo, anthropogenic heat output). Seventeen LCZ classes were determined, ten built types, which depend on the height and density of the buildings, and seven surface cover types. In addition, four more variable land cover properties can be used to refine the LCZ classes. WUDAPT<sup>2</sup> is an international initiative, to collect data on the structure and functioning of cities. Bechtel et al. (2015) created a method, to prepare easily the LCZ maps of the cities. The detailed description of this method and the maps already created by the method are summarized on the WUDAPT's website<sup>3</sup>. Gál et al. (2015) already prepared the LCZ maps of two Hungarian cities, the capital (Budapest) and the third most populated city (Szeged). We use the LCZ map of Budapest in this study. Because of the regional characteristics not all the 17 LCZ classes can be found in Budapest, e.g. LCZ 1 (Compact high-rise buildings) does not appear in the LCZ map of the city. The seven LCZ classes being present in Budapest are as follows:

- LCZ 2: Compact midrise
- LCZ 5: Open midrise
- LCZ 6: Open low-rise
- LCZ 8: Large low-rise
- LCZ A: Dense trees
- LCZ D: Low plants
- LCZ G: Water

We used a 70 × 70 km<sup>2</sup> domain of the MODIS grid cells, which include Budapest and its agglomeration, and transformed the LCZ map of Budapest<sup>4</sup> to this domain (Fig. 20).

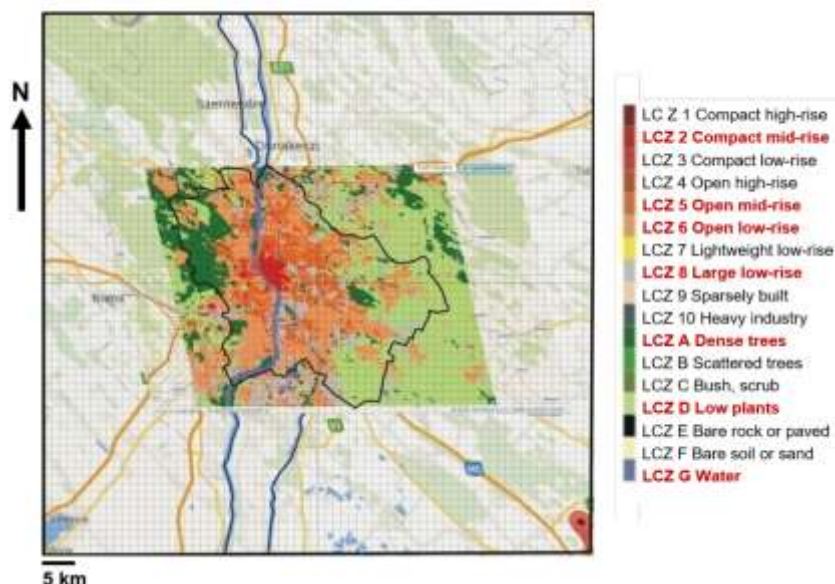


Fig. 20: The local climate zone map of Budapest transformed to the MODIS grid (70×70 km<sup>2</sup> domain). LCZ types appearing in Budapest and its close vicinity are highlighted with red.

<sup>2</sup> World Urban Database and Access Portal Tool

<sup>3</sup> <http://www.wudapt.org/>

<sup>4</sup> [http://geopedia.world/#T4\\_L107\\_x2130299.978307\\_8623\\_y6020180.347740481\\_s11\\_b17](http://geopedia.world/#T4_L107_x2130299.978307_8623_y6020180.347740481_s11_b17)

The main steps of the method are (i) to determine the LCZ class for each MODIS grid cell, (ii) to determine cloud coverage criteria. The first step determines the characteristic LCZ class of each MODIS grid cell (covering 1 km<sup>2</sup>) within the administrative boundaries of Budapest:

LCZ Class criterion 1 (LC1): the dominant LCZ is considered in the grid cell, independently from the extent of the actual coverage of the different LCZ classes present within the grid cell;

LCZ Class criterion 2 (LC2): the LCZ, which covers at least 50% of the grid cell;

LCZ Class criterion 3 (LC3): the LCZ, which covers at least 75% of the grid cell.

Fig. 21 shows the number of grid cells belonging to the given LCZ class for LC1, LC2, LC3 criteria. All the grid cells can be classified according to LC1, and as the criterion becomes stricter, the total number of classified grid cells decrease, thus for example LCZ G cannot be found when using LC3. The maximum number of grid cells belong to LCZ 6 (open low rise) when using LC1 and LC2, and LCZ D (low plants) in LC3. The minimum number of grid cells can occur in LCZ 2 (compact midrise) in the city centre.

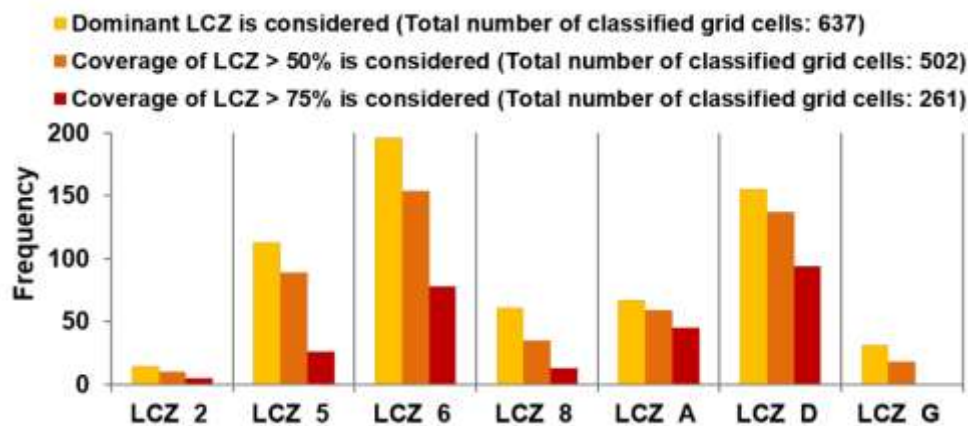


Fig. 21: The distribution of MODIS grid cells according to the LCZ types in Budapest based on the three criteria

The second step determines the cloud cover of each grid cell. The satellite sensors do not measure the land surface temperature in cloudy weather. Three cloud cover criteria are created in this analysis, depending on the extent of cloud cover in the total 70 × 70 km<sup>2</sup> target domain:

Cloud Cover criterion A (CCA): less than 25% of the grid cell is covered with cloud

Cloud Cover criterion B (CCB): less than 10% of the grid cell is covered with cloud

Cloud Cover criterion C (CCC): 0% of the grid cell is covered with cloud  
(i.e. cloudless days)

To analyze the annual distribution of SUHI intensity we used the LC2 and CCA criteria. Terra and Aqua satellites both have two passes over the target area. Fig. 22 summarizes these distributions in each LCZ classes. The evening and dawn LST is determined by long wave radiation, so that is why night-time average SUHI intensities show 1-2 °C variation throughout the whole year for each LCZ class. The day-time SUHI intensity has a substantially different annual distribution because of the shortwave radiation. The highest night-time and day-time intensity can also be found in the most built-up areas of Budapest (LCZ 2). The lowest intensity values occur in low vegetation covered parts of the city (LCZ D) at night, and the lowest day-time SUHI intensities, negative values can be found in LCZ A, the forested areas of Budapest, because these areas of the city are cooler than the rural surroundings.

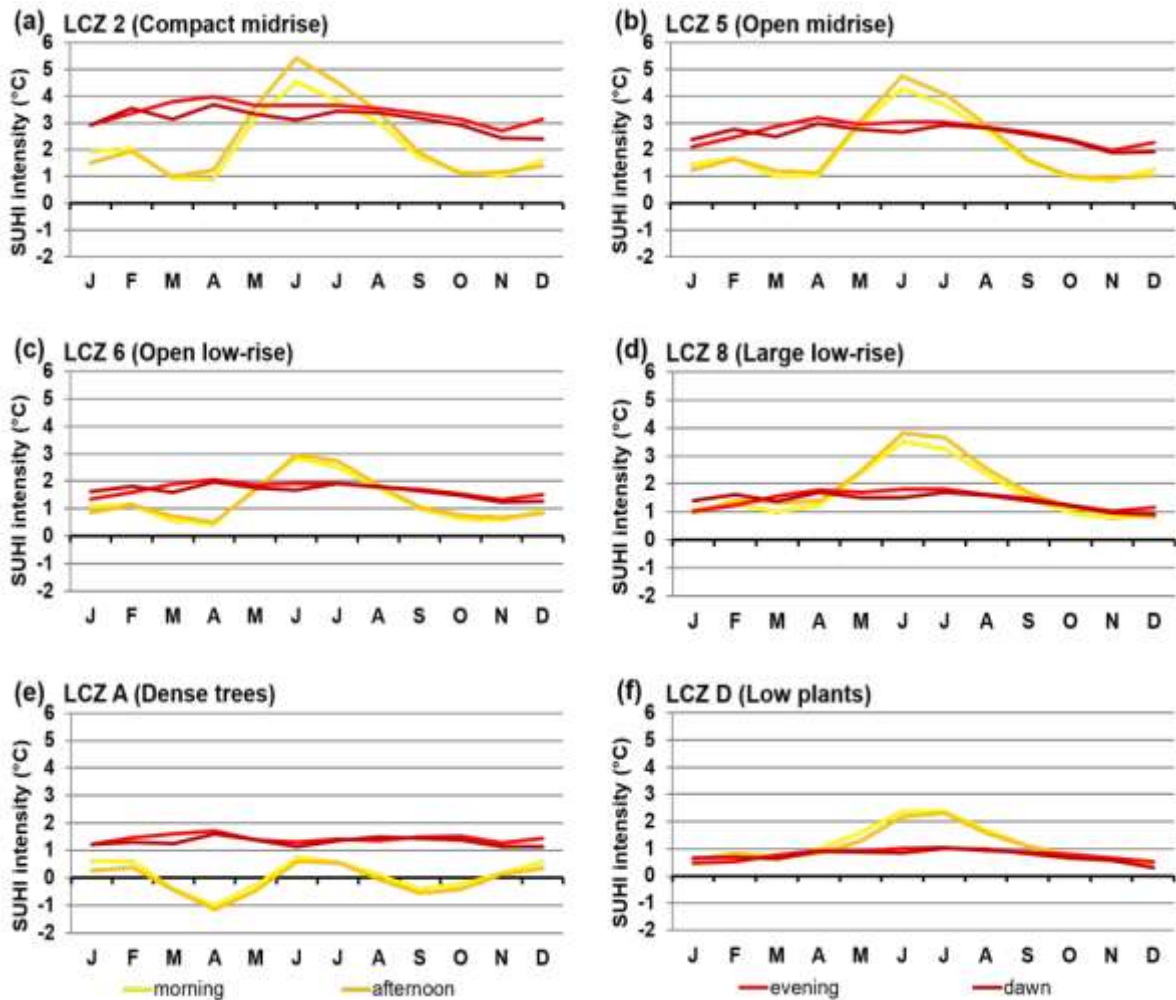


Fig. 22: Annual distribution of monthly mean SUHI intensity averaged over individual LCZ classes during the four satellite measurement times

We used the Aqua’s afternoon measurements to compare the monthly SUHI intensity time series of eight selected grid cells, which are included in the same LCZ class as pairs. Table 3 and Fig. 23 summarize the selected grid cells.

Table 3. The LCZ type, name and location (latitude, longitude) of the selected grid cells

Grid cell	LCZ type	Name (location)
1	LCZ 2: Compact mid-rise	City Center, North (47.5°N, 19.2°E)
2		City Center, South (47.5°N, 19.2°E)
3	LCZ 5: Open mid-rise	Újpest (47.6°N, 19.2°E)
4		Csepel (47.5°N, 19.2°E)
5	LCZ 6: Open low-rise	Kispest (47.5°N, 19.2°E)
6		Budatétény (47.4°N, 19.1°E)
7	LCZ A: Dense trees	Csillebérc (47.5°N, 19.1°E)
8		Budapesti Kamaraerdő (47.4°N, 19.1°E)

The following three criteria were considered for the selection:

- the given LCZ class covers the entire grid cell;
- the grid cells from the same LCZ class should be as far from each other as possible;
- the vicinity of the selected grid cells should belong to the same LCZ class as the selected ones as much as possible.

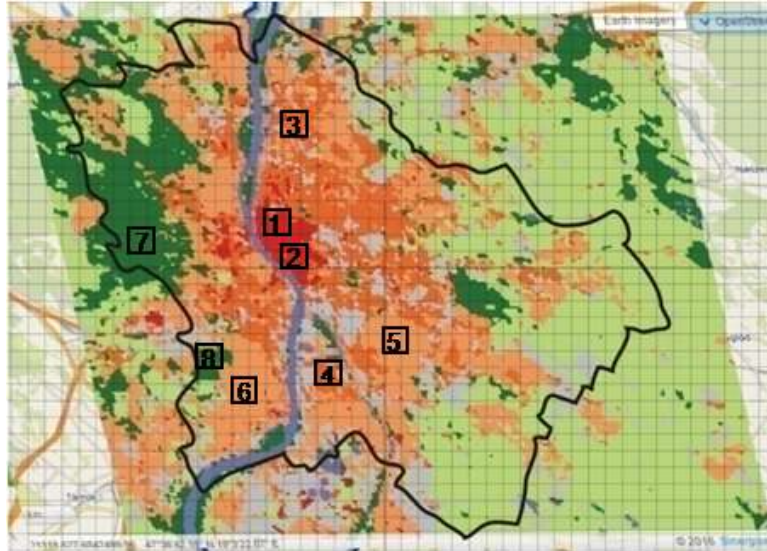


Fig. 23. The location of the grid cells selected for the comparison

To calculate the relationship between the time series we used the linear correlation coefficient ( $r$ ) and the root mean square error (RMSE). Due to their definition, smaller RMSE and greater  $r$  value indicate a greater similarity between the two compared time series.

Table 4. The RMSE values and the correlation coefficient ( $r$ ) of the selected grid cells in each LCZ class

LCZ class	RMSE	$r$
LCZ 2	0.052	0.94
LCZ 5	0.165	0.81
LCZ 6	0.135	0.79
LCZ A	0.208	0.53

Table 4 summarizes the RMSE and  $r$  values for the four compared LCZ classes, and Fig. 24 shows the time series. The smallest RMSE and the greatest correlation can be found in LCZ 2, the city center, where the two selected grid cells are close to each other. Larger differences can be observed in the time series of LCZ 5 and LCZ 6, the RMSE values are greater, and the correlations are smaller than in LCZ 2, due to the different surroundings of the grid cells. The smallest similarity is in LCZ A (Dense trees). The SUHI intensities are mostly negative in these grid cells, due to the geographical location of the grid cells. The Budapesti Kamaraerdő (8) is included in a smaller forest area, and it has a lower height above sea level (100 200 m) than Csillebérc (9) (400 500 m).

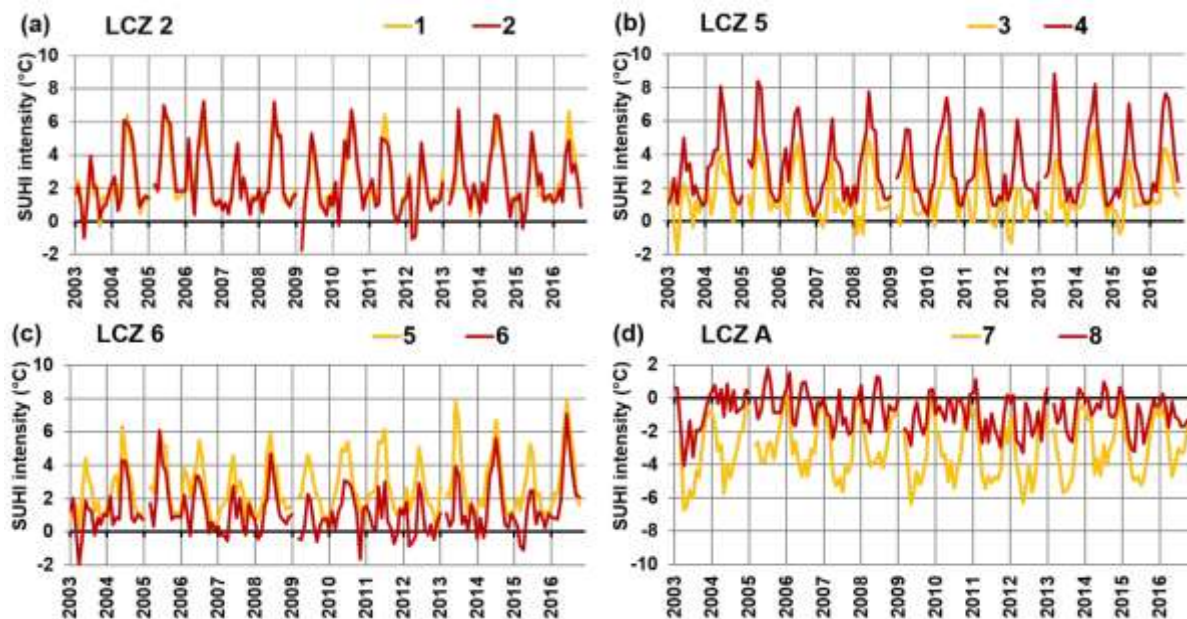


Fig. 24. Comparison of the monthly SUHI intensity time series in the selected grids cells of LCZ 2 (a), LCZ 5 (b), LCZ 6 (c), and LCZ A (d) based on the Aqua afternoon measurements.

The main conclusions can be drawn as follows. The main conclusions of the study are summarized as follows. (1) The highest SUHI intensities clearly occurred in LCZ 2 (compact midrise). (2) When the built-up density decreases, then the SUHI intensities also decrease. (3) The lowest SUHI intensities (negative values) can be found in the vegetation-covered LCZ classes.

The main journal publication of these project results:

Dian Cs., Pongrácz R., Dezső Zs., Bartholy J., (2020): Annual and monthly analysis of surface urban heat island intensity with respect to the local climate zones in Budapest. *Urban Climate*, Vol. 31, 100573. 16p. DOI: 10.1016/j.uclim.2019.100573

#### 4. Modelling approach: UHI and climate change

In addition to the measurements, mesoscale model simulations also have a great potential in analyzing the urban environment, especially, in terms of specific events (Göndöcs et al., 2018). We used the Weather Research and Forecasting (WRF) mesoscale model (Skamarock et al., 2008) coupled to multilayer urban canopy parameterization in our research project to investigate the climatic conditions in their complexity for Budapest and its surroundings. Several possibilities are available in WRF to model the urban environment. The model includes three types of urban parametrization.

(1) The bulk urban parametrization in the so-called Noah scheme, using variant parameters for the urban surfaces (referred as SLAB model). The roughness-length is 0.8 m to represent the drag effects due to buildings, the albedo is 0.15 to represent the shortwave radiation trapping due to urban canyons, and the volumetric heat capacity and thermal conductivity are also different from the natural surface parameters. Furthermore, it calculates the soil moisture and temperature at four levels under the built-up surfaces

(2) A more complex urban parametrization in WRF is the single-layer urban canopy model (SLUCM). The calculations use infinitely-long street canyons parameterized to represent urban geometry. SLUCM recognizes the three-dimensional extension of the cities

resulting in shadowing, radiation trapping, and reflection. The total sensible heat flux involves the fluxes from roof, wall, roads, and added to the calculated sensible heat flux from Noah LSM. Anthropogenic heat and its diurnal variation are predefined in SLUCM, and incorporated by adding them to the sensible heat flux from the urban canopy layer. The presence of the buildings increases the roughness, therefore this scheme calculates the drag effects with exponential wind profile over the city (Fig. 25, left).

(3) One of the most sophisticated urban canopy models in WRF is the BEP (Building Energy Parametrisation), which allows direct interaction with the planetary boundary layer (Fig. 25, right). The three dimensional extent of buildings represent sources and sinks of heat, moisture, and momentum. Prognostic turbulent kinetic energy is generated by the effects of vertical (walls) and horizontal (streets and roofs) surfaces of momentum. The BEP keeps the building internal temperatures constant, in contrast to BEM (Building Energy Model), which takes into account the heat generated by buildings and equipments, such as air conditioning, ventilation, and heating at each floor of the building, which depends on the height of the buildings. BEM calculates the radiation passing through windows and the indoor temperature. The incoming shortwave radiation is reflected, shadowed, and trapped depending on the surface properties and their orientations. The BEP model can be used by itself, or coupled to the BEM model, however, when considering temperature, the BEP alone will perform worse than the SLAB model. To take appropriate use of BEP/BEM, high vertical resolution of the urban canopy is needed. In order to increase the resolution in the urban model, several atmospheric model levels are necessary in the urban canopy layer, which requires dense vertical levelling close to the surface.

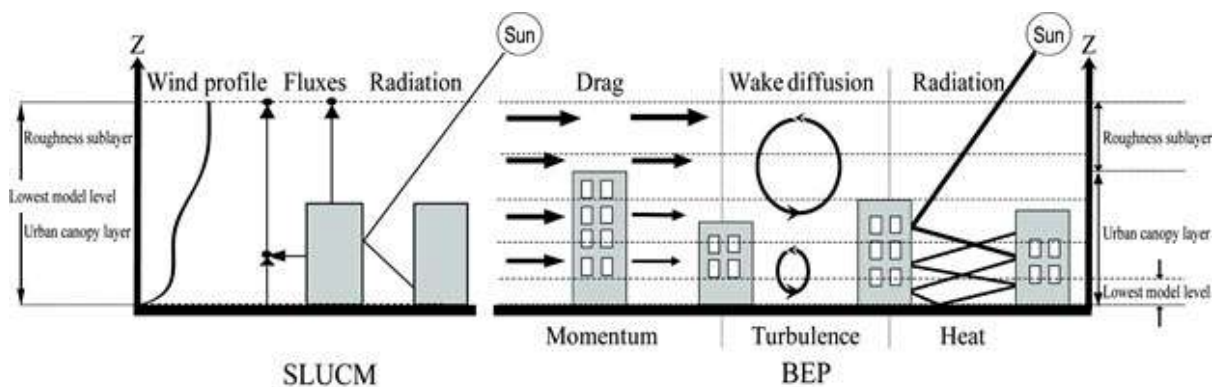


Fig. 25. Schematic effects of urban parameterisations in WRF.

Left: Single-layer urban canopy model, Right: Building Energy Model (Chen et al., 2010).

In our simulations three target areas were defined (Fig. 26a,b), the most external (D01) domain covers the whole Carpathian Basin with 10 km horizontal resolution, whereas the innermost domain (D03) covers Budapest and its surroundings with 1111.11 m grid resolution. The intermediate embedded domain D02 (horizontal resolution: 3333.33 m) is needed for the dynamical downscaling in order to prevent numerical instabilities. All these domains used 44 Eta vertical levels. In order to complete the research study, a high-resolution up-to-date LULC distribution database was generated over the area of Budapest. The editable and freely available online OpenStreetMap<sup>5</sup> (OSM) was used due to the absence of a fine resolution and detailed surface database for Europe within the WRF pre-processing system. It contains different land use categories, water bodies, transport networks and other surface information for the whole world. The available vector and raster files over Budapest and its

<sup>5</sup> <https://www.openstreetmap.org/>

surroundings were downloaded through Mapzen<sup>6</sup> and processed with the QGIS Geographic Information System. The OSM database distinguishes 43 land use categories for Budapest, which we re-categorised in compliance with the 27 Noah land use categories used. Over the area, the necessary LULC information was transformed to a regular grid with an approximately 90 m horizontal resolution to create the binary file needed for the WRF model pre-processing system. The so-called CORINE<sup>7</sup> 2000 database was used to fill the missing land use points. To reproduce a more realistic urban domain, the densely built-up city centre, the artificially covered airport (near the southeastern border of Budapest, within the administrative border, 47°26'N, 19°15'E), and the greenbelt area around Budapest were characterised based on Google Earth satellite images, resulting in five urban surface categories over the city (Fig. 26e).

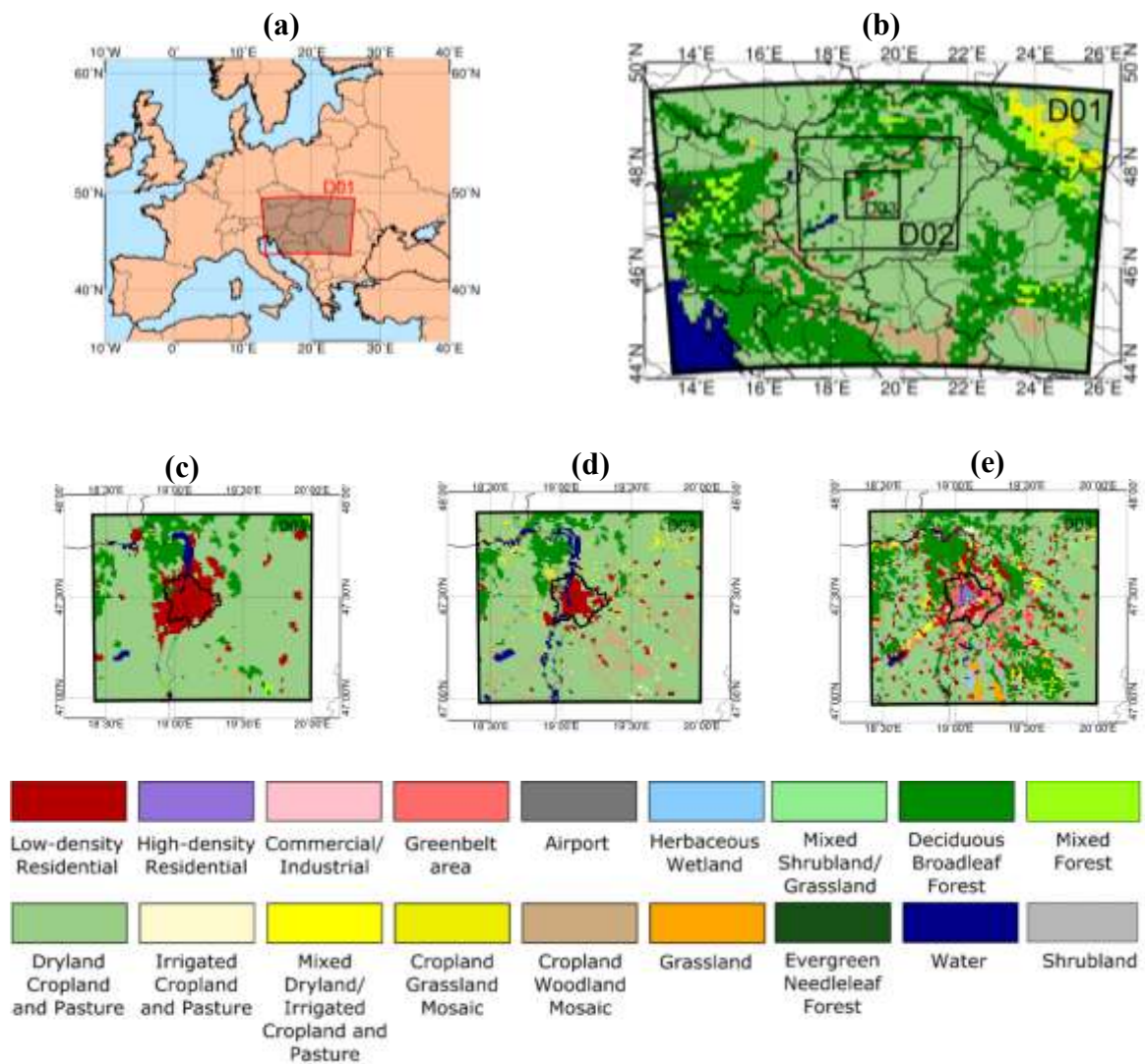


Fig. 26. WRF set-up and land use-land cover maps. The selected D01 domain in Central Europe (a) and its default land use cover within the WRF indicating the embedded D02 and D03 domains (b).

Land use cover maps using different datasets: MODIS land use (c), USGS land use (d), OpenStreetMap land use (e). The black line represents the administrative border of Budapest.

<sup>6</sup> <https://mapzen.com/>

<sup>7</sup> COoRDination of INformation on the Environment

Another option to create the model surface is to use the USGS land use database (Fig. 26d), originally found in the WRF pre-processing system, which was developed using the AVHRR<sup>8</sup> derived NDVI<sup>9</sup> composites from April 1992 through March 1993 with a resolution of 1 km. This contains only one single urban surface category, and therefore it is not able to reproduce the inhomogeneity of urban areas. After the WRF model version 3.1 another alternative LULC dataset was released, which was retrieved from the 2001 MODIS satellite products (Fig. 26c). The dataset includes one single urban category similarly to the USGS LULC dataset, but it categorises the surface imprecisely over the course of the Danube and in urbanised areas. Moreover, as it can be seen in Figs. 26c and 26d, the extent of Budapest is not precise at all in these cases unlike in the newly compiled dataset. Aside from city structure, the rural areas are also substantially different. On the one hand, urban area does not appear within the agglomeration area of Budapest in the USGS dataset, and is substantially reduced in the MODIS dataset. On the other hand, the OSM land use-land cover dataset includes the most deciduous broadleaf forest coverage (26%) compared to 8.3% for the USGS and 10% for MODIS datasets. As Fig. 26c shows, the MODIS surface cover contains three main categories (low-density residential (41.8%), dryland cropland and pasture (45.2%), and deciduous broadleaf forest (10.2%)), while the USGS database is supplemented by the cropland woodland mosaic category (6.6%). The OSM is more detailed, thus it has more categories (grassland and extended urban classes) than the others.

For the winter and summer simulations the initial meteorological fields were derived from the publicly available GFS (Global Forecast System) outputs for the past, and a regional climate model (RegCM) for the future (Piecza et al., 2018). To validate the simulation results, the calculated skin temperature over Budapest was compared (Göndöcs et al., 2017) to the surface temperature fields of the remotely sensed measurements of sensor MODIS. Moreover, the simulated air temperature fields were also evaluated, and special locations were selected to analyze the temporal evolution of UHI effect in details. RegCM-driven WRF simulations were analyzed to provide information for different users (including decision makers) on the future UHI effects of the Budapest agglomeration under different RCP scenarios (van Vuuren et al., 2011).

For the validation experiments, the different surface databases were tested. The spatial distributions of the surface temperature and the 2-m air temperature are presented in Fig. 27. The higher temperatures are associated with a higher PBL and greater SH, while the vegetated and water-covered (course of the Danube in the USGS and MODIS land use) areas with higher LH reduce these temperatures. Compared to the others the WRF/OSM simulation shows warmer areas around the city both in the near-surface air and surface temperature fields, but the city structure shows a more realistic picture, with a warm centre and outward radial pattern of temperature decrease. The WRF/MODIS and WRF/USGS simulations result in almost equal average surface temperatures around Budapest (16–18 °C) and within the city 21–22 °C. The most marked difference between the spatial distributions of surface temperature is the course of the Danube flowing through Budapest (breadth is overestimated), nevertheless in the further UHI/SUHI calculations these pixels were not used. The bottom row of Fig. 27 shows the 2-m average temperature fields at night, and the pictures clearly show the analysed UHI phenomenon. Both simulations generated warm(er) urban areas, however, the UHI intensities are not equal in all cases. The WRF/MODIS simulation generated the greatest night time UHI intensity (2.13 °C), and the WRF/OSM the weakest (1.59 °C).

---

<sup>8</sup> Advanced Very High Resolution Radiometer

<sup>9</sup> Normalised Difference Vegetation Index

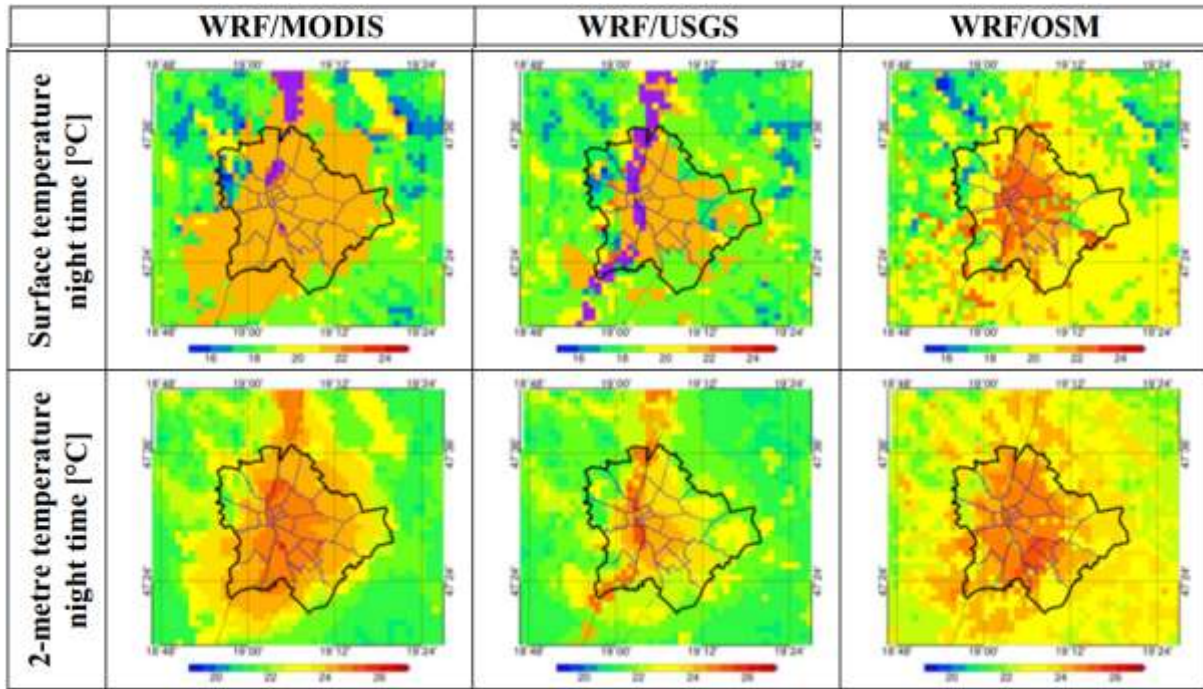


Fig. 27. Daytime or night time averages of surface temperature (top) and 2-m air temperature (bottom).

Contrary to the satellite measurements, which are available only four times a day, the model provides the surface temperature every 15 minutes. A close relationship can be mostly found between the SUHI and UHI, although some important differences should be mentioned. UHI intensities, i.e. the air temperature difference between the built-up areas and their surroundings is greater at night and smaller during the day, with the opposite being true for SUHI intensities based on skin temperature. Fig. 28 summarises the hourly variability of SUHI intensities (shaded areas) for each simulation. The diurnal SUHI variation has its first maximum when the incoming shortwave radiation directly reaches the surface. Around sunset, the planetary boundary layer collapses due to the reduced turbulent kinetic energy, and thus, the SUHI intensities slowly decrease. After sunset the city becomes warmer again, due to the large volumetric heat capacity, conductivity and emissivity of the built-up areas. In parallel with the previous results, the WRF/MODIS simulation resulted in the strongest SUHI (with an average intensity of 3.2 °C), and higher variability throughout the week, with 0.65 °C during the day and 0.43 °C at night. The WRF/USGS and WRF/OSM simulations generated quite similar intensities, with average values of 1.8 °C and 1.6 °C, respectively. Their weekly variabilities are lower (0.39 °C for both simulations) than the variability of the WRF/MODIS simulation. During the daylight hours the SUHI of the WRF/OSM simulation is weaker than the SUHI of the WRF/USGS simulation due to the warmer surroundings and cooler city. Fig. 28 also shows the SUHI values calculated from satellite data during overpasses when the cloud cover over the Bp\_dom area does not exceed 30 percent. The SUHI intensities from the satellite observations are closer to the WRF/MODIS at night, in contrast to the daylight hours, when the measurements are dispersed more between the three simulated datasets.

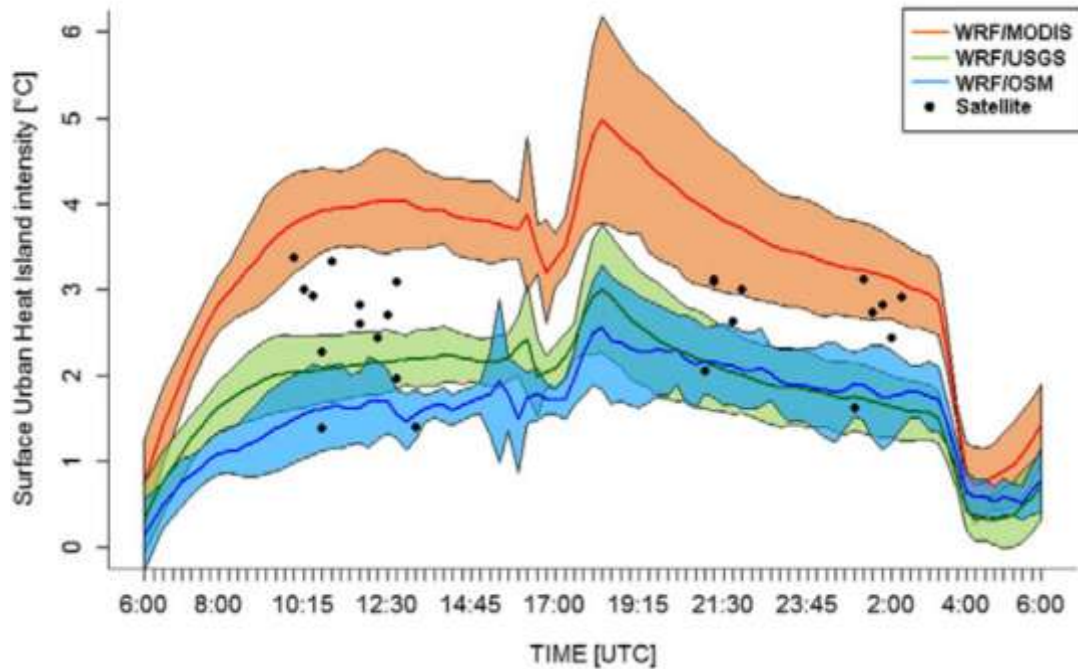


Fig. 28. The hourly variability of the SUHI intensities compared to the intensity values calculated from available satellite measurements.

The conclusions of the research study with three WRF-simulations are as follows. When the full Bp\_dom area was taken into account without any restrictions during the RMSE calculation, the results from the WRF/OSM showed best agreement with the observations both in rural and urban areas, in contrast to the WRF/USGS, which resulted in the greatest errors. According to the mean normalised bias calculations, the WRF/OSM simulation estimated the lowest bias in urban areas, although an overestimation was detected over the surrounding rural areas, which resulted in weaker SUHI intensity. In general, the model was able to reproduce the magnitude of SUHI well, however, it performed better during the night than during the day. When using the OSM LULC database, the model reproduced the most realistic SUHI structure in Budapest, although it underestimated its intensity. This underestimation can be explained by the overestimation of skin temperature over rural areas. This was partially caused by the inadequate heat exchange calculation over forests. Although the WRF/USGS simulation resulted in similar RMSE values both for TSK and SUHI than the WRF/OSM simulation, the rural areas were colder in the former simulation, resulting in higher SUHI intensity.

The main journal publications of these project results:

- Göndöcs J., Breuer H., Pongrácz R., Bartholy J. (2017): Urban heat island mesoscale modelling study for the Budapest agglomeration area using the WRF model. *Urban Climate*, 21, pp. 66-86. DOI 10.1016/j.uclim.2017.05.005
- Göndöcs J., Breuer H., Pongrácz R., Bartholy J. (2017): Városi hősziget meghatározásának lehetőségei a WRF modell felhasználásával. *Légtér* 62. (No. 4.) pp. 165-170. (in Hungarian)
- Göndöcs J., Breuer H., Pongrácz R., Bartholy J. (2018): Projected changes in heat wave characteristics in the Carpathian Basin comparing different definitions. *Int. Journal of Global Warming*. Vol. 16 (No.2.) pp.119-135. DOI 10.1504/IJGW.2018.10015777
- Dian Cs., Talamon A., Pongrácz R., Bartholy J. (2021): Analysis of the heating and cooling periods in Budapest using station data. *Időjárás*, 125 (No. 3.) pp. 431-448. DOI: 10.28974/idojaras.2021.3.4

## References

- Bartholy, J., Pongrácz, R., Dezső, Zs., Dian, Cs., Fricke, C., 2016: Recent changes on the urban local climate using satellite data and in-situ measurements. In: *96th Annual Meeting of the American Meteorological Society*. New Orleans, LA. Paper 873, 8p. Available online at [https://ams.confex.com/ams/96Annual/webprogram/Manuscript/Paper285360/Extended-paper-BJ-PR-DZs-DCS-FC\\_2016\\_AMS.pdf](https://ams.confex.com/ams/96Annual/webprogram/Manuscript/Paper285360/Extended-paper-BJ-PR-DZs-DCS-FC_2016_AMS.pdf)
- Bechtel, B., Alexander, P. J., Böhner, J., Ching, J., Conrad, O., Feddema, F., Mills, G., See, L., Stewart I. D., 2015. Mapping Local Climate Zones for a Worldwide Database of the Form and Function of Cities. *ISPRS International Journal of Geo-Information*, 4, 199–219. DOI: 10.3390/ijgi 4010199
- Gál T., Bechtel B., Unger J., 2015. Comparison of two different Local Climate Zone mapping methods. *ICUC9 conference extended abstracts*. Toulouse, France, 20-24.07.2015. Paper: [http://www.meteo.fr/icuc9/LongAbstracts/gd2-6-1551002\\_a.pdf](http://www.meteo.fr/icuc9/LongAbstracts/gd2-6-1551002_a.pdf)
- Göndöcs, J., Breuer, H., Pongrácz, R., Bartholy, J., 2017: Urban heat island mesoscale modelling study for the Budapest agglomeration area using the WRF model. *Urban Climate*, 21, 66–86.
- Göndöcs, J., Breuer, H., Pongrácz, R., Bartholy, J., 2018: Projected changes in heat wave characteristics in the Carpathian Basin comparing different definitions. *International Journal of Global Warming*, 16, 119–135.
- LGF, Local Government of Ferencváros, 2010: Rehabilitation of Budapest Ferencváros. Budapest, 80p.
- NASA, 1999: Science writers' guide to Terra. NASA EOS Project Science Office, Greenbelt, MD. 28p.
- NASA, 2002: Science writers' guide to Aqua. NASA EOS Project Science Office, Greenbelt, MD. 32p.
- Pieczka, I., Pongrácz, R., Bartholy, J., Szabóné André, K., 2018: Future temperature projections for Hungary based on RegCM4.3 simulations using new representative concentration pathways scenarios. *International Journal of Global Warming*, 15, 277–292.
- Pongrácz, R., Bartholy, J., Dezső, Zs., 2006: Remotely sensed thermal information applied to urban climate analysis. *Advances in Space Research*, 37, 2191-2196.
- Pongrácz, R., Bartholy, J., Dezső, Zs., 2010: Application of remotely sensed thermal information to urban climatology of Central European cities. *Physics and Chemistry of Earth*, 35, 95–99.
- Pongrácz, R., Bartholy, J., Dezső, Zs., Dian, Cs., 2016: Analysis of the air temperature and relative humidity measurements in the Budapest Ferencváros district. *Hungarian Geographical Bulletin*, 65, 93-103. DOI: 10.15201/hun geobull.65.2.1
- Pongrácz, R., Bartholy, J., Dian Cs., Dezső, Zs., 2018: Intra-annual characteristics of the relationship between the surface temperature based urban heat island intensity and the local climatic zones. *98th Annual Meeting of the American Meteorological Society*. Austin, TX. Paper 569, 6p. Available online at <https://ams.confex.com/ams/98Annual/webprogram/Manuscript/Paper336512/PR-BJ-DCs-DZs-AMS2018.pdf>
- Skamarock, W.C., Klemp, J.B., Dudhia, J., Gill, D.O., Barker, D.M., Duda, M.G., Huang, X.-Y., Wang, W., Powers, J.G., 2008: A Description of the Advanced Research WRF Version 3. NCAR/TN–475+STR, June 2008. – NCAR Technical Note.

- Stewart, I.D., Oke, T.R., 2012: Local Climate Zones for urban temperature studies. *Bulletin of the American Meteorological Society*, 93, 1879–1900. DOI: 10.1175/BAMS-D-11-00019.1
- van Vuuren, D.P., Edmonds, J.A., Kainuma, M., Riahi, K., Thomson, A.M., Hibbard, K., Hurtt, G.C., Kram, T., Krey, V., Lamarque, J.-F., Masui, T., Meinshausen, M., Nakicenovic, N., Smith, S.J., Rose, S., 2011: The representative concentration pathways: an overview. *Climatic Change*, 109, 5–31.
- Wan, Z., Snyder, W., 1999: MODIS land-surface temperature algorithm theoretical basis document. Inst. for Computational Earth Systems Science, Univ. of California, Santa Barbara. 77p.